Oil Shale, 2022, Vol. 39, No. 3, pp. 169–188
doi: https://doi.org/10.3176/oil.2022.3.02

Experimental investigation on the hydrocarbon generation of low maturity organic-rich shale in supercritical water

Tian Xie[(a)], Qiuyang Zhao[(a)*], Yu Dong[(a)], Hui Jin[(a,b)], Yechun Wang[(a,b)], Liejin Guo[(a)*]

[(a)] State Key Laboratory of Multiphase Flow in Power Engineering, Xi'an Jiaotong University, Xi'an 710049, China
[(b)] Xinjin Weihua Institute of Clean Energy Research, Foshan City, 528216, China

Received 18 April 2022, accepted 15 July 2022, available online 10 September 2022

Abstract. *In this study, the hydrocarbon generation of 1–4 cm sized shale in supercritical water (SCW) was investigated. The results showed that temperature was the most important factor affecting the hydrocarbon generation of organic-rich shale in the presence of supercritical water. In the temperature range of 380–450 °C, the optimum oil generation temperature was 430 °C. The produced oil component became heavier with increasing temperature. Increasing temperature was beneficial to gas production and improved the selectivity of H_2 and CH_4. In the pressure range of 22.5–27.5 MPa, oil and gas production decreased with increasing pressure. The influence of pressure on conversion path was almost negligible. Pressure affected the hydrocarbon generation of shale in supercritical water by affecting hydrocarbon expulsion. In the water-shale mass ratio range of 0.5–5 and the reaction time range of 1–12 h, increasing both parameter ranges was conducive to the hydrocarbon generation of oil shale. The selectivity of H_2 increased and that of CH_4 and CO_2 decreased with increasing water-shale mass ratio. The selectivity of CH_4 and C_2H_6 increased with increasing reaction time.*

Keywords: *organic-rich oil shale, supercritical water, hydrocarbon generation, conversion.*

* Corresponding authors: e-mails *qyzhao@mail.xjtu.edu.cn; lj-guo@mail.xjtu.edu.cn*

1. Introduction

Organic matter mainly exists in the form of kerogen in low maturity organic-rich shale, and the bottleneck to its utilization is how to accelerate the conversion of kerogen into oil and gas [1, 2]. The presence of water brings many changes to the hydrocarbon generation of organic-rich shale [3].

Supercritical water (SCW) is water above its critical points (374 °C and 22.1 MPa) [4], and it has excellent physical and chemical properties such as high reactivity, solubility and diffusion. A large number of studies have shown that supercritical water has good effects and broad application prospects in biomass degradation [5–8], organic waste treatment [9–12], clean utilization of coal [13–15] and heavy oil development [16–21]. Supercritical water provides two paths for the treatment of the above mixtures of macromolecular organic matter [22–27]. One is rapid pyrolysis to produce oil, and the other is direct gasification to produce hydrogen-rich syngas. Supercritical water can not only realize the effective utilization of the above resources, but also remove chlorine, sulfur, nitrogen elements, etc., and reduce the discharge of toxic and harmful substances in the treatment of macromolecular organic matter.

In recent years, many scholars [28–34] reported that kerogen can be converted into light oil in supercritical water atmosphere, and the distribution of conversion products, influencing factors and conversion mechanism were studied. The conversion products mainly include oil and gas phase substances. The main controlling factors of shale hydrocarbon generation include temperature, pressure, water-shale mass ratio and reaction time. In previous studies, due to the coupling influence of temperature, pressure and water-shale mass ratio, the strict control of a single variable was often not achieved. For example, when temperature factor was studied, the usual method was to control the constant quality of shale and water added, which actually caused pressure to increase with temperature. In the study of pressure factor, the usual method was to control the constant temperature and the mass of shale, and increased the mass of water to achieve the final pressure increase, which in fact also increased the water-shale mass ratio. In essence, the hydrocarbon generation of kerogen in supercritical water is mainly caused by the rupture and recombination of C–C, C–O, C–N, C–S bonds, etc.

Hu et al. [28] found that the extracted products were mainly asphaltenes, and the natural gas generation rate reached the maximum at 390 °C. Veski et al. [29] studied the co-pyrolysis hydrocarbon generation process of kukersite oil shale and pine in supercritical water, and found that the content of polar components in co-pyrolysis oil production was higher than that in single shale oil production. Funazukuri et al. [30] established that oil production under supercritical water atmospheres had a higher content of small molecular component at 435 °C than at 380 °C. Yanik et al. [31] and El Harfi et al. [32] found that water could react with olefin to generate alcohols and aldehydes. Fedyaeva et al. [33] explored a new approach to treating sulfur-containing oil

shale with SCW to obtain ideal sulfur-containing products. Nasyrova et al. [34] discovered that the conversion of kerogen was the result of the fracture of C–C, C–N and C–O bonds. Recently, some scholars studied the law of supercritical water gasification of low maturity organic-rich shale to produce hydrogen-rich syngas. Liang et al. [35] found the optimal working conditions to be the following: temperature 700 °C, pressure 22.1 MPa, water/shale mass ratio 5:1, time 4 h and particle size range 10–20 mesh.

Overall, previous studies focused more on the mechanism of conversion reaction, grinding the shale used in the experiment into as small particles as possible (0–3 mm), so that it can fully react in supercritical water. However, there is still no noteworthy report on co-pyrolysis hydrocarbon generation of centimeter sized low maturity organic-rich shale and supercritical water.

In this paper, a non-isothermal heating reactor and a method for controlling a single variable were used to simulate the hydrocarbon generation process of the 1–4 cm sized low maturity organic-rich shale in the presence of supercritical water. The effects of temperature (T = 380–450 °C), pressure (P = 22.5–27.5 MPa), water-shale mass ratio (R = 0.5–5) and reaction time (t = 1–12 h) on hydrocarbon generation efficiency and product characteristics were investigated.

2. Experimental section

2.1. Experimental method and procedure

All experiments were carried out in a 80 mL non-isothermal heating reactor, which was made of Hastelloy alloy, at a maximum temperature of 600 °C and a maximum pressure of 35 MPa. The heating rate was 4 °C/min. In this study, the temperature factor was investigated by increasing or decreasing the mass of added water to realize the constant pressure in the temperature increasing process. Accordingly, in order to keep the water-shale mass ratio unchanged, the mass of added rock also increased or decreased respectively. The pressure factor was studied by changing the quality of added water. At the same temperature, in order to keep the water-shale mass ratio constant after the change of water quality, the mass of added shale also increased or decreased accordingly. The study of water-shale mass ratio was achieved by keeping the water mass constant and changing the shale mass.

The experimental procedure was carried out as follows:

Step 1: The required amounts of shale (M_{shale}) and deionized water (M_{water}) were added in the reactor. Thereafter, the argon water was used to discharge air inside the reactor.

Step 2: For the detection of any possible leaks, the reactor pressure was suppressed to a value of 2 MPa. Once the sealing of the reactor was confirmed to be intact, the pressure inside the reactor was released to atmospheric pressure.

Step 3: The heating device was opened and when the reactor temperature reached the design temperature, the preset reaction timer was started. After the lapse of desired time, the reactor in water was quenched to bring it towards ambient temperature.

Step 4: The reactor was opened for collection of gas phase products. The total gas volume was measured with a wet gas flowmeter and sampled into an air bag for further analysis. The gas volume is expressed in the units of V_{gas}.

Step 5: Both solid and liquid from the reactor were placed inside a centrifugal bottle, and an appropriate amount of CS_2 for the purpose of centrifugation was added. Once the centrifugation was complete, the centrifuge bottle was composed of water layer, CS_2 extraction layer and solid residue from top to bottom.

Step 6: All three components were separated by placing the CS_2 extraction solution in a drying oven at 46 °C. The CS_2 produced oil was dried, measured and denoted in the units of M_{oil}. The solid residue was also placed in a drying oven at 100 °C, its mass was weighed and expressed in $M_{residue}$.

Step 7: The oil, gas and solid residues were thoroughly tested and analyzed. Each step of the experiment was repeated twice and the average value of the two experiments was considered for calculations to ensure the experimental accuracy.

2.2. Materials and analytical methods

The low maturity organic-rich shale was recovered from the well F317-181 in Ordos Basin, China. Its characteristics are presented in Table 1. The experimental material used in this study were shale samples with a size of 1–4 cm. The oil products were measured using an Agilent 7890b chromatograph, an Elementar vario Macro cube on CHNS mode elemental analyzer and an IATROSCAN MK-6S chromatograph equipped with a flame ionization detector. The gas products were analyzed using an Agilent 7890a gas chromatograph equipped with a thermal conductivity detector and a flame ionization detector. The total carbon (TC) and total organic carbon (TOC) of the solid residue after the reaction were measured by an Elementar vario MACRO cube. According to the test results, the organic carbon contents of original oil shale and corresponding semi-cokes were calculated, which were denoted by $M_{toc\text{-}shale}$ and $M_{toc\text{-}residue}$, respectively. In this paper, organic carbon utilization (Eq. (1)), oil production (Eq. (2)) and gas production (Eq. (3)) were used to evaluate the conversion effect, which were denoted by W_{toc}, W_{oil} and W_{gas}, respectively:

$$W_{toc} = \left(1 - \frac{M_{(toc-residue)}}{M_{(toc-shale)}}\right) \times 100\%, \tag{1}$$

$$W_{oil} = \frac{M_{oil}}{M_{shale}} \times 100\%, \tag{2}$$

$$W_{gas} = V_{gas}/M_{shale}. \tag{3}$$

Table 1. The properties of oil shale sample used in the study

Proximate analysis, air dried basis, wt%		Ultimate analysis, dried basis, wt%		Fischer assay analysis, received basis, wt%	
Moisture	1.56	C*	16.42	Shale oil	5.32
Ash	72.69	H	1.55	Water	4.75
Volatile matter	10.53	N	1.07	Semi-coke	83.67
Fixed carbon	15.22	S	5.13	Gas + loss	6.26

* Total organic carbon obtained by pickling is 16.25 wt%

3. Results and discussion

3.1. Effect of temperature

Table 2 shows the utilization of organic carbon and production of shale oil and gas at different temperatures ranging from 380 to 450 °C. With the reaction temperature increasing from 380 to 450 °C, W_{toc} and W_{oil} increased first and then decreased, reaching the maximum 15.89% and 0.42% at 430 °C, respectively. This indicates that increasing temperature before 430 °C was beneficial to the hydrocarbon generation of shale in supercritical water, and the further increase of temperature after 430 °C would be part of the converted organic matter secondary coking. W_{gas} increased from 10.80 to 36.02 mL/g. This indicates that the gasification of low maturity organic-rich shale in supercritical water was promoted by increasing temperature. There are two reasons for the decrease of W_{oil} after 430 °C with temperature. One is that the coking of oil production occurs with the further increase of temperature during the release from the shale to the outer space, and the other is that the increase of temperature promotes the conversion of released oil to gas.

Figure 1a shows that in the range of 380–450 °C, the relative contents of saturated and aromatic hydrocarbon in oil decreased and those of resin and asphaltene increased with increasing temperature. Figure 1c reveals that the carbon numbers in oil ranged mainly from C_8 to C_{56}. The fractions below C_{16} decreased with temperature, while the fractions above C_{16} increased with

temperature. Figure 1d demonstrates the content of carbon in oil to increase and that of hydrogen to decrease with temperature. It can be inferred that the ratio of hydrogen to carbon atoms decreased with temperature. These results indicate that the produced oil component of 1–4 cm shale became heavier with increasing temperature. However, Funazukuri et al. [30] found that the relative content of heavy components of oil produced by the 0.35–0.84 mm shale decreased with increasing temperature. The reason for this is that the conversion mechanism of shale in supercritical water includes anhydrous and aqueous conversion mechanism. For the pore areas that can be swept by supercritical water, organic matter can directly contact with water. Supercritical water not only plays a physical heating role, but also participates in conversion reaction as reactant. Zhao et al. [36] discovered that supercritical water could effectively inhibit the coking of heavy oil. For the pore areas that cannot be swept by supercritical water, it only plays a physical heating role, and organic matter conversion in the pore area is essentially similar to destructive distillation. Savage et al. [37] established that asphaltenes from California coast crude oil pyrolysis at 400 °C had a coking induction period, but when the pyrolysis temperature increased to 450 °C, the coking induction period disappeared and the asphaltenes coking took place in a very short time. Shale is a kind of dense rock, and the increase of shale size makes it difficult for supercritical water to penetrate into the internal pores of shale deeply and contact with organic matter directly. Therefore, anhydrous conversion mechanism is the main control mechanism in this study.

The hydrocarbon generation path of low maturity organic-rich shale usually includes the conversion of kerogen to oil and gas, and conversion of oil to gas [38]. The change of gas composition is the result of the dual pyrolysis of kerogen and oil. As shown in Figure 1b, with the increase of temperature, the relative contents of H_2 and CH_4 increased, while those of CO_2 and C_2H_4 decreased. The relative contents of C_2H_6 and C_{3+} increased first and then decreased with temperature. This indicates that the large hydrocarbon macromolecules in the gas generated from the initial pyrolysis of solid organic matter would crack again with the further increase of temperature, and CH_4 molecules would be the main final product.

The main sources of H_2 are organic matter pyrolysis reaction, steam-reforming reaction (Eq. (4)) and water-gas shift reaction (Eq. (5)) [39]. Water-gas shift reaction is kinetically favored at high temperature [18]. Therefore, higher temperature would lead to higher hydrogen selectivity by promoting the steam-reforming reaction and accelerating the water-gas shift reaction:

$$C + H_2O \rightarrow CO + H_2;\ \Delta H = 131.31 \frac{kJ}{mol}, \tag{4}$$

$$CO + H_2O \rightarrow CO_2 + H_2;\ \Delta H = -41.15 \frac{kJ}{mol}. \tag{5}$$

Both methanation reaction [9, 39] and organic matter pyrolysis reaction can generate methane. Methanation reaction is an exothermic reaction, and increasing temperature is not conducive to the forward shift of reaction equilibrium. However, increasing temperature promotes the cracking of organic macromolecules in gas, so the increase of methane selectivity with temperature should be attributed to the latter.

CO_2 comes from water shift reaction, carbonate decomposition [40–43], and decarboxylation reaction of carboxyl intermediates and esters [44, 45]. In fact, the yield of CO_2 was almost unchanged with temperature in this study, and the increase of organic components yield in the gas was the main reason for the decrease of CO_2 selectivity.

Overall, there was a peak oil production temperature of 430 °C for the organic-rich shale in Ordos Basin. For the 1–4 cm sized shale, increasing temperature would increase the polymerization tendency of oil production and promote the selectivity of H_2 and CH_4.

Table 2. Evaluation index statistics of conversion efficiency at different temperatures

Index	380 °C	410 °C	430 °C	450 °C
W_{toc}, %	2.65	11.08	15.89	11.41
W_{oil}, %	0.13	0.39	0.42	0.08
W_{gas}, mL/g	10.80	16.87	33.27	36.02

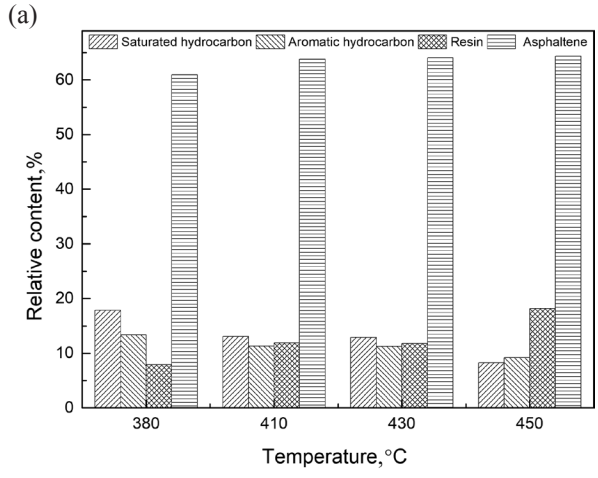

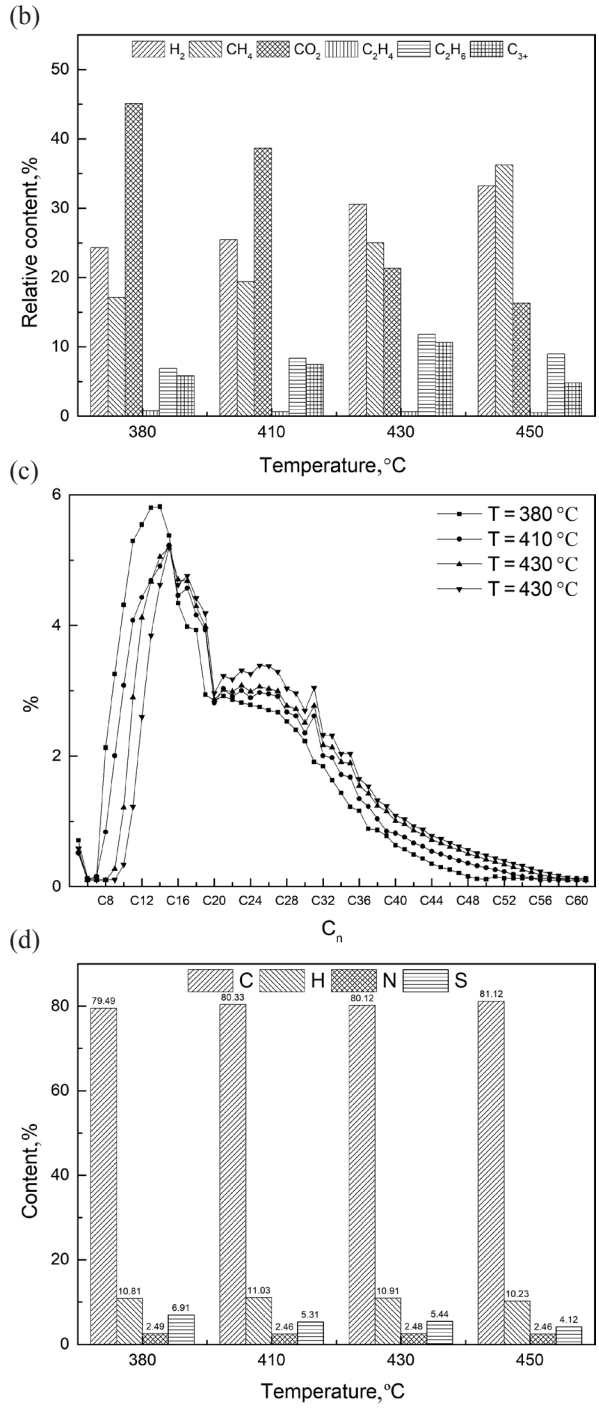

Fig. 1. Effect of temperature on product composition: (a) oil products composition; (b) gas products composition; (c) carbon number distribution of oil; (d) ultimate analysis of oil. These experiments were performed at a pressure of 24 MPa, a water-shale mass ratio of 1:1 and a total heating time of 2.5 h.

3.2. Effect of pressure

Table 3 shows the utilization of organic carbon and production of shale oil and gas at different pressures ranging from 22.5 to 27.5 MPa. With pressure increasing from 22.5 to 27.5 MPa, the utilization of organic carbon and production of oil and gas decreased, from 5.69 to 5.19%, 0.24 to 0.15%, and 15.64 to 14.99 mL/g, respectively. As shown in Figures 2a, 2b, 2c and 2d, the relative contents of oil components and gas components, carbon number distribution and ultimate analysis data of oil products remained constant with pressure. This indicates that increasing pressure inhibits hydrocarbon expulsion and has almost no effect on the reaction path. Therefore, it can be inferred that the pressure mainly affects the hydrocarbon generation of shale in supercritical water through affecting the hydrocarbon expulsion process.

Table 3. Evaluation index statistics of conversion efficiency at different pressures

Index	22.5 MPa	24.5 MPa	26 MPa	27.5 MPa
W_{toc}, %	5.69	5.32	5.24	5.19
$W_{oil,}$, %	0.24	0.22	0.21	0.15
W_{gas}, mL/g	15.64	15.26	15.00	14.99

(a)

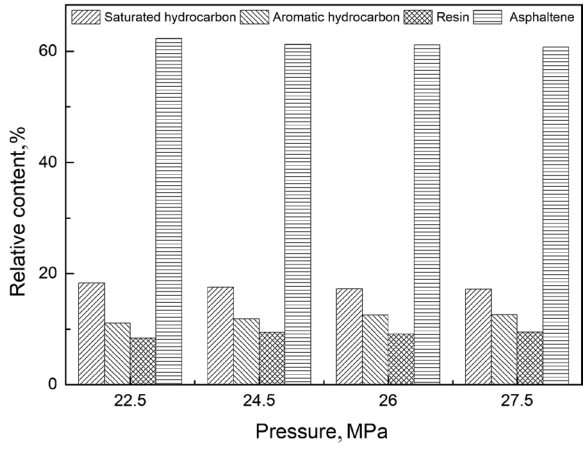

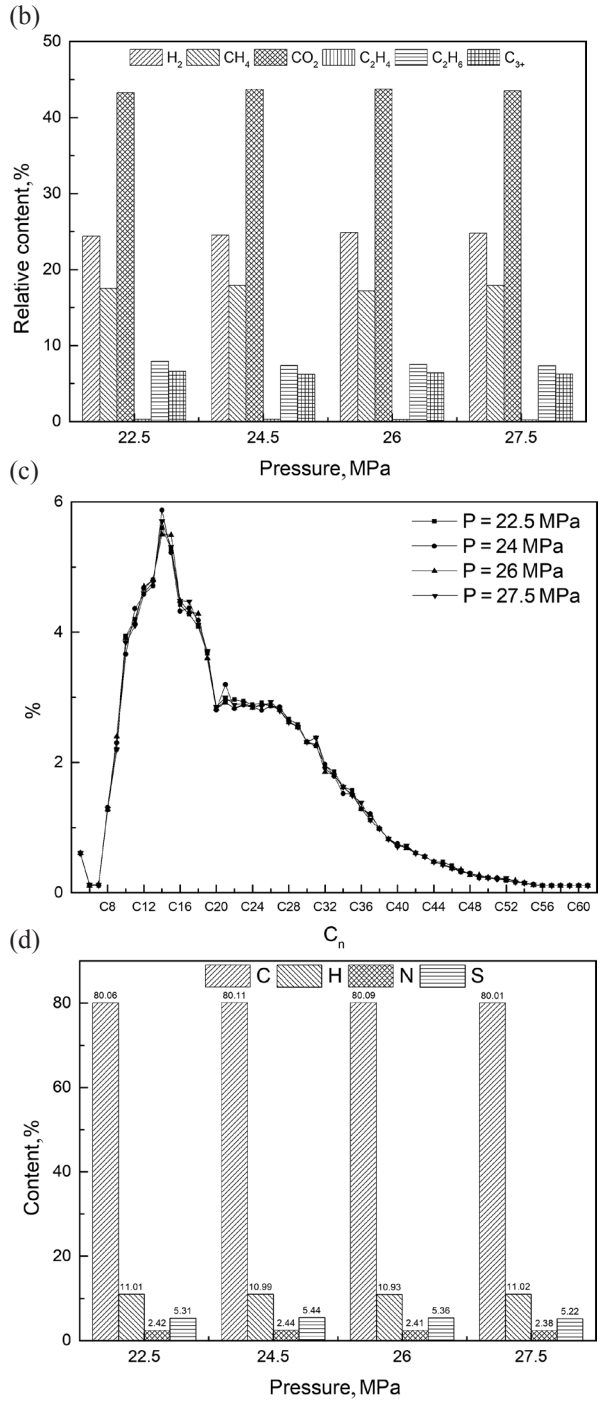

Fig. 2. Effect of pressure on product composition: (a) oil products composition; (b) gas products composition; (c) carbon number distribution of oil; (d) ultimate analysis of oil. These experiments were performed at a temperature of 400 °C, a water-shale mass ratio of 1:1 and a reaction time of 1 h.

3.3. Effect of water-shale mass ratio

Table 4 shows the utilization of organic carbon and production of shale oil and gas at different water-shale mass ratios ranging from 0.5 to 5. With water-shale mass ratio increasing from 0.5 to 5, the organic carbon utilization increased from 4.86 to 6.25%, oil production from 0.20 to 0.41% and gas production from 14.13 to 25.37 mL/g. As shown in Figure 3a, with the increase of water-shale mass ratio, the relative content of asphaltene decreased, while those of saturated hydrocarbon, aromatic hydrocarbon and resin increased. Figure 3c shows that the content of small carbon atoms in oil products increased with the increase of water-shale mass ratio. Figure 3d displays the content of carbon in oil products to decrease and that of hydrogen to increase with water-shale mass ratio. It can be inferred that the ratio of hydrogen to carbon atoms increased with water-shale mass ratio. These results prove that the light components of oil increased with the increase of water-shale mass ratio. In this study, the water-shale mass ratio was varied by changing the quality of added shale and keeping that of added water unchanged. Therefore, the increase of water-shale mass ratio is actually equivalent to the decrease of shale size. Hydrocarbons within shale are more easily captured by supercritical water. Figure 3b demonstrates that the relative contents of H_2 and CO_2 increased, while that of CH_4 decreased. Overall, increasing water-shale mass ratio was favorable to the release of organic matter in shale and improved the proportion of light components in oil. The selectivity of H_2 increased and that of CH_4 and CO_2 decreased with increasing water-shale mass ratio.

Table 4. Evaluation index statistics of conversion efficiency at different water-shale mass ratios

Index	0.5	1	2	5
W_{toc}, %	4.86	5.29	5.81	6.25
W_{oil}, %	0.20	0.22	0.35	0.41
W_{gas}, mL/g	14.13	15.15	19.66	25.37

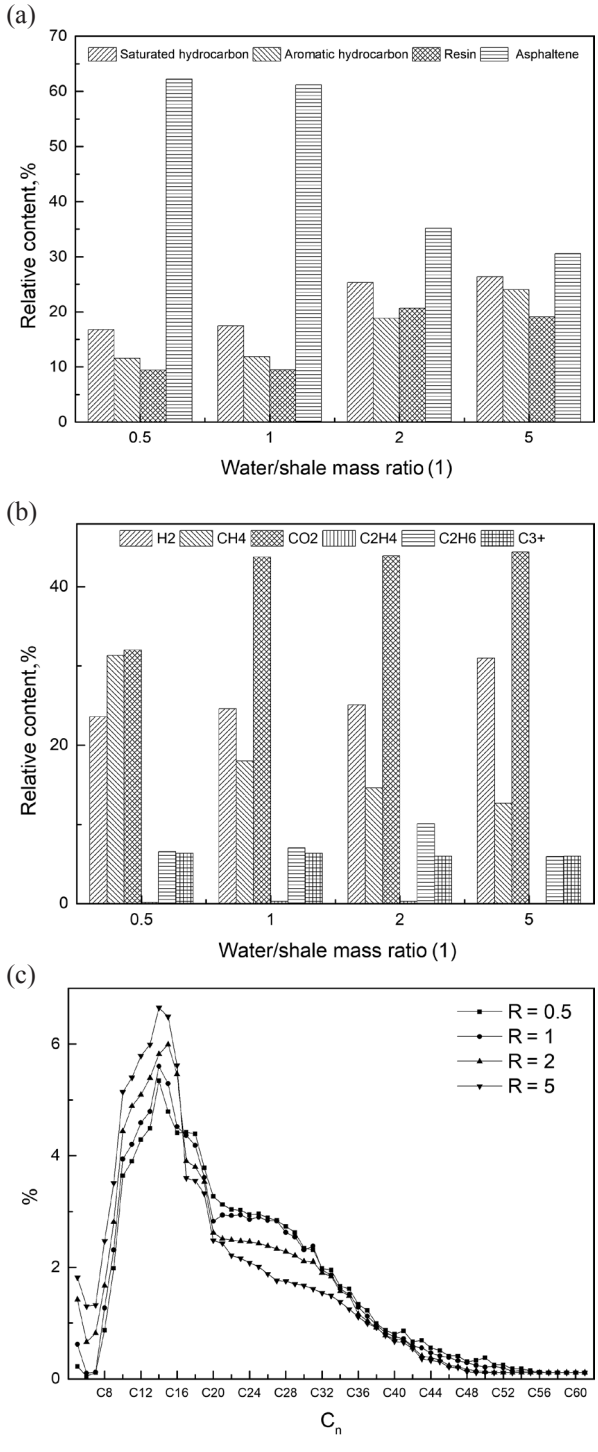
(a)
Saturated hydrocarbon
Aromatic hydrocarbon
Resin
Asphaltene
Relative content,%
Water/shale mass ratio (1)
(b)
H2
CH4
CO2
C2H4
C2H6
C3+
Relative content,%
Water/shale mass ratio (1)
(c)
R = 0.5
R = 1
R = 2
R = 5
%
C8 C12 C16 C20 C24 C28 C32 C36 C40 C44 C48 C52 C56 C60
Cn

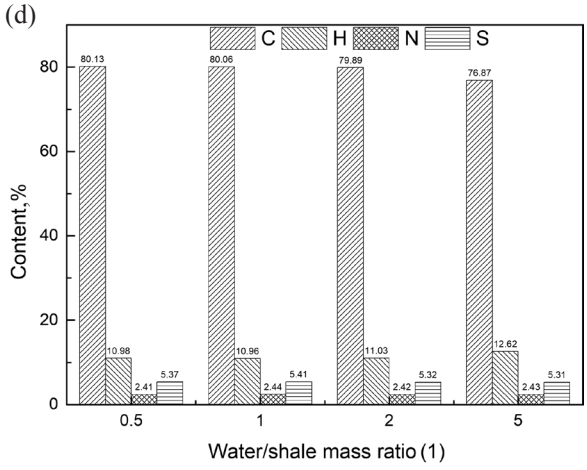

Fig. 3. Effect of water-shale mass ratio on product composition. (a) oil products composition; (b) gas products composition; (c) carbon number distribution of oil; (d) ultimate analysis of oil. These experiments were performed at a temperature of 400 °C, a pressure of 25 MPa and a reaction time of 1 h.

3.4. Effect of reaction time

Table 5 shows the utilization of organic carbon and production of shale oil and gas at different reaction times ranging from 1 to 12 h. With reaction time increasing from 1 to 12 h, the organic carbon utilization increased from 5.41 to 16.93%, production of oil first increased and then decreased, reaching a maximum, 0.37%, at 4 h, and the production of gas increased from 15.43 to 27.57 mL/g. Figure 4a shows that with the increase of reaction time, the relative contents of saturated hydrocarbon, aromatic hydrocarbon and resin increased, while that of asphaltene decreased. Figure 4c reveals that the relative content of small carbon atoms of oil increased with the increase of reaction time. Figure 4d displays the relative contents of carbon and hydrogen of oil to increase with reaction time. As demonstrated in Figure 4b, the relative contents of CH_4 and C_2H_6 increased with the increase of reaction time. This indicates that the large molecules of gas would be re-cracked with the increase of reaction time. Overall, in the range of 1–12 h, increasing reaction time could improve the release of organic matter in shale pores. Although increasing reaction time could increase the light components of oil, it would promote converting oil to gas. The selectivity of small molecular hydrocarbons (CH_4, C_2H_6) increased with the increase of reaction time.

Table 5. Evaluation index statistics of conversion efficiency at different reaction times

Index	1 h	4 h	8 h	12 h
W_{toc}, %	5.41	7.41	11.31	16.93
W_{oil}, %	0.22	0.37	0.32	0.16
W_{gas}, mL/g	15.43	17.22	21.66	27.57

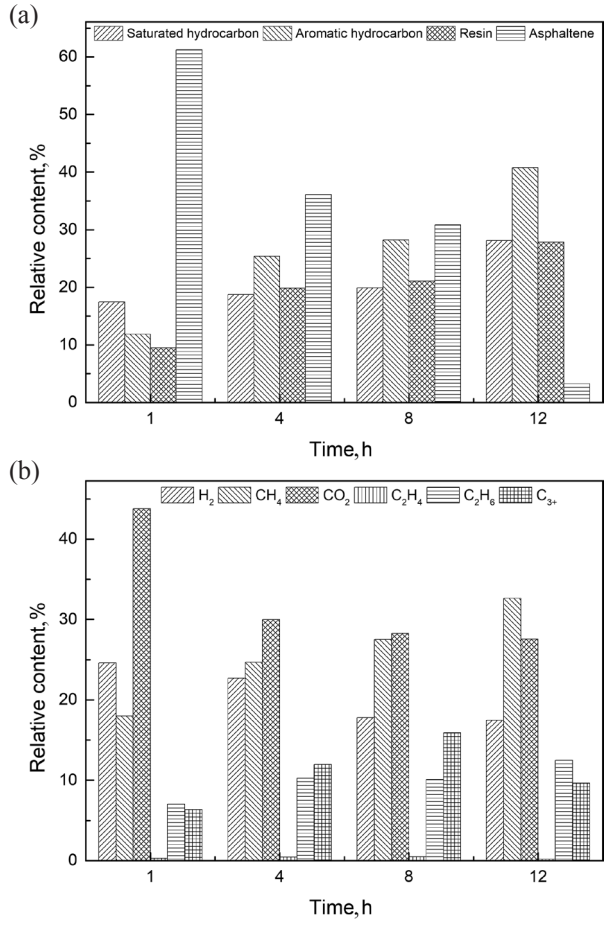

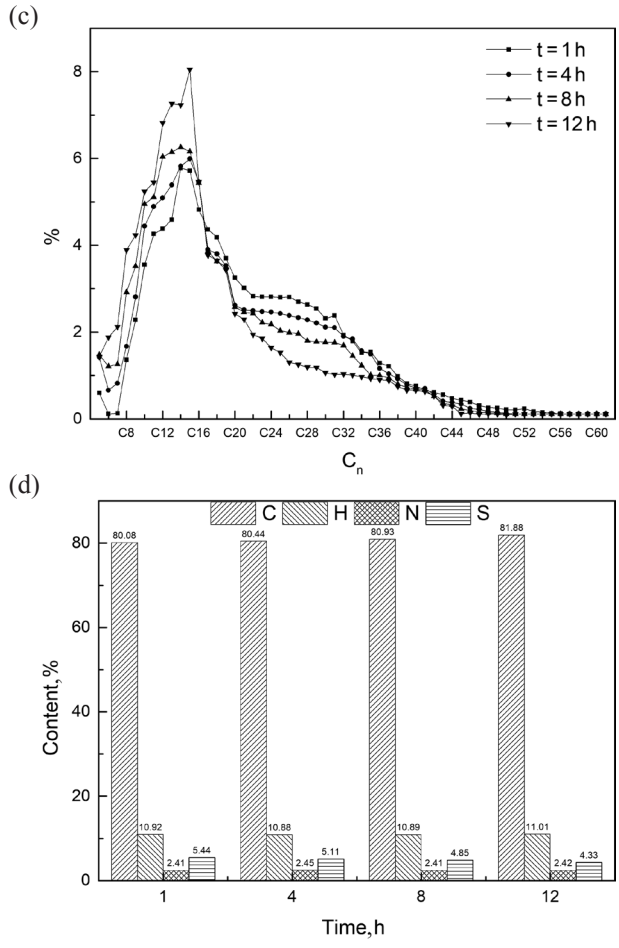

Fig. 4. Effect of reaction time on product composition: (a) oil products composition; (b) gas products composition; (c) carbon number distribution of oil; (d) ultimate analysis of oil. These experiments were performed at a temperature of 400 °C, a pressure of 24 MPa and a water-shale mass ratio of 1:1.

3.5. Comparing the results with findings of previous studies

A comparative analysis of the results of this work and literature sources was conducted to elucidate the respective hydrocarbon generation characteristics. The main operating conditions and experimental results are given in Table 6. As seen from Table 6, when the temperature increased, the oil production rate first increased and then decreased with a peak at about 430 °C and the gas production rate continued to increase. The other operating parameters and shale particle size remained unaffected. As increasing temperature promoted both the decomposition of kerogen into oil and that of oil into gas, so, when oil consumption exceeded its generation, oil production reached a peak. In

addition, high temperature also accelerated the reactions of steam reforming, water-gas shift and methanation, increasing thus the selectivity of H_2 and CH_4. It is worth noting that the light fraction content in produced oil increased with temperature for small shale particles of 0.35–0.84 mm [30], while the heavy fraction content increased for large shale particles of 10–40 mm in this work. Supercritical water is more likely to enter the interior of small particles and dissolve heavy fraction to form miscibility [16], thus promoting decomposition and inhibiting polymerization. Obviously, the time extension had a similar effect as increasing temperature, that is, promoted both organic matter conversion and secondary decomposition of produced oil because there existed a peak oil production rate and continuously increasing gas production rate. Table 6 shows the effect of pressure on product distribution to be negligible. It was also found that increasing water-shale mass ratio improved oil and gas production. It is to be noted that an increase in water-shale mass ratio referred to the smaller size of shale particles in this work. This could promote heat and mass transfer, accelerate oil and gas generation and shorten oil and gas migration from shale particle interior to supercritical water, resulting in the increase of oil and gas production.

Table 6. Hydrocarbon generation characteristics of shale in supercritical water

	Experimental conditions	Main results	
		Cause	Results
Hu [28]	P = 30 MPa, T = 360–450 °C, φ = 2–2.5 mm	T↑	W_{oil}↑↓, peaking at 425 °C; W_{gas}↑
El Harfi [32]	P = 25 MPa, T = 400 °C, R = 5, t = 1.17–1.48 h, Φ = 1–1.25mm	t↑	W_{oil}↑; W_{gas}↑
Funazukuri[30]	P = 23 MPa, T = 380–400 °C, R = 12.5, t = 0–1 h, φ = 0.35–0.84 mm	T↑	W_{oil}↑↓, peaking at 437–457 °C, Heavy fraction↓
		t↑	W_{oil}↑; W_{gas}↑
This work	P = 22.5–27.5 MPa, T = 380–450 °C, R = 0.5–5, t = 1–12 h, φ = 10–40 mm	T↑	W_{oil}↑↓, peaking at 430 °C, Heavy fraction of oil↑ W_{gas}↑, selectivity of H_2↑ and CH_4↑
		P↑	W_{oil}↓, W_{gas}↓, oil/gas composition unchanged
		t↑	W_{oil}↑↓, peaking at 4 h; W_{gas}↑
		R↑	W_{oil}↑; W_{gas}↑

Note: The symbols of "↑" and "↓" represent increase and decrease, respectively; "W_{oil}" represents oil production; "W_{gas}" represents gas production; "T" represents reaction temperature; "P" represents pressure; "t" represents reaction time; "R" represents water-shale mass ratio; "φ" represents shale size.

4. Conclusions

In this study, a non-isothermal heating reactor was used to simulate the hydrocarbon generation low maturity organic-rich shale in the presence of supercritical water. The effects of temperature, pressure, water-shale mass ratio and reaction time were investigated. The main conclusions are as follows.

1. In the temperature range of 380–450 °C, the optimum oil generation temperature was 430 °C. The content of heavy components in oil increased with increasing temperature. Increasing temperature was beneficial to gas production and improved the selectivity of H_2 and CH_4.
2. In the pressure range of 22.5–27.5 MPa, oil and gas production decreased with pressure increasing. The influence of pressure on conversion path was negligible. Pressure affected hydrocarbon generation of shale in supercritical water by affecting hydrocarbon expulsion.
3. In the water-shale mass ratio range of 0.5–5 and the reaction time range of 1–12 h, increasing water-shale mass ratio and reaction time was conducive to the hydrocarbon generation of oil shale, and promoted the gasification of oil shale semi-coke.

Acknowledgments

The financial support by the Basic Science Center Program of the Ordered Energy Conversion of the National Nature Science Foundation of China (No. 51888103), the China Postdoctoral Science Foundation funded project (No. 2020M683476), and the Fundamental Research Funds for the Central Universities are gratefully acknowledged.

REFERENCES

1. Mozaffari, S., Järvik, O., Baird, Z. S. Composition of gas from pyrolysis of Estonian oil shale with various sweep gases. *Oil Shale*, 2021, **38**(3), 215–227.
2. Jin, Z., Bai, Z., Gao, B., Li, M. Has China ushered in the shale oil and gas revolution? *Oil Gas Geol.*, 2019, **40**(3), 451–458.
3. Tang, X., Li, S., Yue, C., He, J., Hou, J. Lumping kinetics of hydrodesulfurization and hydrodenitrogenation of the middle distillate from Chinese shale oil. *Oil Shale*, 2013, **30**(4), 517–535.
4. Hermann, W., Ernst, U. F. Supercritical water as a solvent. *Angew. Chem. Int. Ed.*, 2005, **44**(18), 2672–2692.
5. Kruse, A. Supercritical water gasification. *Biofuel. Bioprod. Biorefin.*, 2008, **2**(5), 415–437.
6. Reddy, S. N., Nanda, S., Dalai, A. K., Kozinski, J. A. Supercritical water gasification of biomass for hydrogen production. *Int. J. Hydrog. Energy*, 2014, **39**(13), 6912–6926.

7. Rodriguez Correa, C., Kruse, A. Supercritical water gasification of biomass for hydrogen production – Review. *J. Supercrit. Fluids*, 2018, **133**, Part 2, 573–590.
8. Oasmaa, A., Lehto, J., Solantausta, Y., Kallio, S. Historical review on VTT fast pyrolysis bio-oil production and upgrading. *Energy Fuels*, 2021, **35**(7), 5683–5695.
9. Xu, J., Kou, J., Guo, L., Jin, H., Peng, Z., Ren, C. Experimental study on oil-containing wastewater gasification in supercritical water in a continuous system. *Int. J. Hydrog. Energy*, 2019, **44**(30), 15871–15881.
10. García-Jarana, M. B., Sánchez-Oneto, J., Portela, J. R., Martínez de la Ossa, E. J. Supercritical water gasification of organic wastes for energy generation. In: *Supercritical Fluid Technology for Energy and Environmental Applications* (Anikeev, V., Fan, M., Eds.). Elsevier: Boston, 2014, 191–200.
11. Wang, W., Lu, H., Wei, W., Shi, J., Zhao, Q., Jin, H. Experimental investigation on the production of hydrogen from discarded circuit boards in supercritical water. *Int. J. Hydrog. Energy*, 2022. https://doi.org/10.1016/j.ijhydene.2021.11.208
12. Wang, C., Zhu, C., Huang, J., Li, L., Jin, H. Enhancement of depolymerization slag gasification in supercritical water and its gasification performance in fluidized bed reactor. *Renew. Energ.*, 2021, **168**, 829–837.
13. Guo, L., Jin, H., Lu, Y. Supercritical water gasification research and development in China. *J. Supercrit. Fluids*, 2015, **96**, 144–150.
14. Xia, F., Tian, S., Ning, P., Gu, J., Guan, Q., Miao, R., Wang, Y. Catalytic gasification of lignite with KOH in supercritical water. *Can. J. Chem. Eng.*, 2014, **92**(3), 421–425.
15. Lan, R., Jin, H., Guo, L., Ge, Z., Guo, S., Zhang, X. Hydrogen production by catalytic gasification of coal in supercritical water. *Energy Fuels*, 2014, **28**(11), 6911–6917.
16. Zhao, Q., Guo, L., Huang, Z., Chen, L., Jin, H., Wang, Y. Experimental investigation on enhanced oil recovery of extra heavy oil by supercritical water flooding. *Energy Fuels*, 2018, **32**(2), 1685–1692.
17. Dejhosseini, M., Aida, T., Watanabe, M., Takami, S., Hojo, D., Aoki, N., Arita, T., Kishita, A., Adschiri, T. Catalytic cracking reaction of heavy oil in the presence of cerium oxide nanoparticles in supercritical water. *Energy Fuels*, 2013, **27**(8), 4624–4631.
18. Rana, R., Nanda, S., Kozinski, J. A., Dalai, A. K. Investigating the applicability of Athabasca bitumen as a feedstock for hydrogen production through catalytic supercritical water gasification. *J. Environ. Chem. Eng.*, 2018, **6**(1), 182–189.
19. Rana, R., Nanda, S., Maclennan, A., Hu, Y., Kozinski, J. A., Dalai, A. K. Comparative evaluation for catalytic gasification of petroleum coke and asphaltene in subcritical and supercritical water. *J. Energy Chem.*, 2019, **31**, 107–118.
20. Liu, J., Xing, Y., Chen, Y., Yuan, P., Cheng, Z., Yuan, W. Visbreaking of heavy oil under supercritical water environment. *Ind. Eng. Chem. Res.*, 2018, **57**(3), 867–875.
21. Ates, A., Azimi, G., Choi, K. H., Green, W. H., Timko, M. T. The role of catalyst in supercritical water desulfurization. *Appl. Catal. B*, 2014, **147**, 144–155.

22. Yu, J., Sun, L., Ma, C., Qiao, Y., Yao, H. Thermal degradation of PVC: A review. *Waste Manage.*, 2016, **48**, 300–314.
23. Yamaguchi, D., Sanderson, P. J., Lim, S., Aye, L. Supercritical water gasification of Victorian brown coal: Experimental characterisation. *Int. J. Hydrog. Energy*, 2009, **34**(8), 3342–3350.
24. Guo, L., Jin, H. Boiling coal in water: Hydrogen production and power generation system with zero net CO_2 emission based on coal and supercritical water gasification. *Int. J. Hydrog. Energy*, 2013, **38**(29), 12953–12967.
25. Li, X., Wu, Z., Wang, H., Jin, H. The effect of particle wake on the heat transfer characteristics between interactive particles in supercritical water. *Chem. Eng. Sci.*, 2022, **247**, 117030.
26. Li, Y., Wang, H., Shi, J., Cao, C., Jin, H. Numerical simulation on natural convection and temperature distribution of supercritical water in a side-wall heated cavity. *J. Supercrit. Fluids*, 2022, **181**, 105465.
27. Lu, Y., Wang, Z., Kang, Z., Li, W., Yang, D., Zhao, Y. Comparative study on the pyrolysis behavior and pyrolysate characteristics of Fushun oil shale during anhydrous pyrolysis and sub/supercritical water pyrolysis. *RSC Advances*, 2022, **12**, 16329–16341.
28. Hu, H., Zhang, J., Guo, S., Chen, G. Extraction of Huadian oil shale with water in sub- and supercritical states. *Fuel*, 1999, **78**(6), 645–651.
29. Veski, R., Palu, V., Kruusement, K. Co-liquefaction of kukersite oil shale and pine wood in supercritical water. *Oil Shale*, 2006, **23**(3), 236–248.
30. Funazukuri, T., Yokoi, S., Wakao, N. Supercritical fluid extraction of Chinese Maoming oil shale with water and toluene. *Fuel*, 1988, **67**(1), 10–14.
31. Yanik, J., Yüksel, M., Saglam, M., Olukcu, N., Bartle, K., Frere, B. Characterization of the oil fractions of shale oil obtained by pyrolysis and supercritical water extraction. *Fuel*, 1995, **74**(1), 46–50.
32. El Harfi, K., Bennouna, C., Mokhlisse, A., Ben Chanâa, M., Lemée, L., Joffre, J., Amblès, A. Supercritical fluid extraction of Moroccan (Timahdit) oil shale with water. *J. Anal. Appl. Pyrolysis*, 1999, **50**(2), 163–174.
33. Fedyaeva, O. N., Antipenko, V. R., Dubov, D. Yu., Kruglyakova, T. V., Vostrikov, A. A. Non-isothermal conversion of the Kashpir sulfur-rich oil shale in a supercritical water flow. *J. Supercrit. Fluids*, 2016, **109**, 157–165.
34. Nasyrova, Z. R., Kayukova, G. P., Onishchenko, Y. V., Morozov, V. P., Vakhin, A. V. Conversion of high-carbon Domanic shale in sub- and supercritical waters. *Energy Fuels*, 2020, **34**(2), 1329–1336.
35. Liang, X., Zhao, Q., Dong, Y., Guo, L., Jin, Z., Liu, Q. Experimental investigation on supercritical water gasification of organic-rich shale with low maturity for syngas production. *Energy Fuels*, 2021, **35**(9), 7657–7665.
36. Zhao, Q., Guo, L., Wang, Y., Jin, H., Chen, L., Huang, Z. Enhanced oil recovery and in situ upgrading of heavy oil by supercritical water injection. *Energy Fuels*, 2020, **34**(1), 360–367.
37. Savage, P. E., Klein, M. T., Kukes, S. G. Asphaltene reaction pathways. 3. Effect of reaction environment. *Energy Fuels*, 1988, **2**(5), 619–628.

38. Campbell, J. H., Koskinas, G. J., Gallegos, G., Gregg, M. Gas evolution during oil shale pyrolysis. 1. Nonisothermal rate measurements. *Fuel*, 1980, **59**(10), 718–726.
39. Susanti, R. F., Veriansyah, B., Kim, J.-D., Kim, J., Lee, Y.-W. Continuous supercritical water gasification of isooctane: A promising reactor design. *Int. J. Hydrog. Energy*, 2010, **35**(5), 1957–1970.
40. Schubert, M., Regler, J. W., Vogel, F. Continuous salt precipitation and separation from supercritical water. Part 1: Type 1 salts. *J. Supercrit. Fluids*, 2010, **52**(1), 99–112.
41. Onsager, O.-T., Brownrigg, M. S. A., Lødeng, R. Hydrogen production from water and CO via alkali metal formate salts. *Int. J. Hydrog. Energy*, 1996, **21**(10), 883–885.
42. Sınağ, A., Kruse, A., Rathert, J. Influence of the heating rate and the type of catalyst on the formation of key intermediates and on the generation of gases during hydropyrolysis of glucose in supercritical water in a batch reactor. *Ind. Eng. Chem. Res.*, 2004, **43**(2), 502–508.
43. Ge, Z., Guo, L., Jin, H. Catalytic supercritical water gasification mechanism of coal. *Int. J. Hydrog. Energy*, 2020, **45**(16), 9504–9511.
44. Wagner, W., Kretzschmar, H.-J. *IAPWS Industrial Formulation 1997 for the Thermodynamic Properties of Water and Steam. International Steam Tables: Properties of Water and Steam Based on the Industrial Formulation IAPWS-IF97*. Springer: Berlin, Heidelberg, 2008, 7–150.
45. Lewan, M. D. Water as a source of hydrogen and oxygen in petroleum formation by hydrous pyrolysis. *Preprints of Papers Presented at the 204th American Chemical Society Meeting*. Washington, D.C., Aug 23–28, 1992, **37**(4), 1643–1649.